

# Simplified Vibration Model and analysis of a single-conductor transmission line with dampers

Proc IMechE Part C:  
J Mechanical Engineering Science  
2017, Vol. 231(22) 4150–4162  
© IMechE 2016  
Reprints and permissions:  
sagepub.co.uk/journalsPermissions.nav  
DOI: 10.1177/0954406216660736  
journals.sagepub.com/home/pic



O Barry<sup>1</sup>, R Long<sup>1</sup> and DCD Oguamanam<sup>2</sup>

## Abstract

A novel model is developed for a vibrating single-conductor transmission line carrying Stockbridge dampers. Experiments are performed to determine the equivalent viscous damping of the damper. This damper is then reduced to an equivalent discrete mass-spring-mass and viscous damping system. The equations of motion of the model are derived using Hamilton's principle and explicit expressions are determined for the frequency equation, and mode shapes. The proposed model is verified using experimental and finite element results from the literature. This proposed model excellently captures free vibration characteristics of the system and the vibration level of the conductor, but performs poorly in regard to the vibration of the counterweights.

## Keywords

Aeolian vibration, Strouhal frequency, messenger, Stockbridge damper, equivalent viscous damping, mass-spring-damper

Date received: 4 August 2015; accepted: 14 March 2016

## Introduction

Aeolian vibration of transmission lines has been a subject of study for many years. It occurs at what is commonly referred to as Strouhal frequency which is proportional to the wind speed and inversely proportional to the diameter of the conductor. The Strouhal frequency varies between 3 Hz and 150 Hz and causes a peak-to-peak amplitude of up to one conductor diameter.<sup>1</sup> Stockbridge dampers are often employed to dampen Aeolian vibration. Their effectiveness is dependent on their position on the conductor, their overall characteristics, and the characteristics of the conductor.

The model of a conductor can be idealized as an axially loaded Euler-Bernoulli beam subjected to an exciting force by the damper. Claren and Diana<sup>2</sup> were among the earliest investigators to examine Aeolian vibration of transmission lines. They analytically and experimentally determined the natural frequencies of the conductor without damping. The effect of the conductor flexural rigidity on natural frequencies was investigated by Dhotard et al.<sup>3</sup> The differences in the values of natural frequencies observed in the simply supported end cable (with and without flexural rigidity) were less than 3%. They hypothesized that the location of the dampers had negligible effect on the strain for low frequency excitation (i.e. low wind speed). Barbieri et al.<sup>4</sup> performed free vibration

analysis of a single conductor without damping using Galerkin method and experimentally validated their results. Barry et al.<sup>5,6</sup> used the finite element (FE) method to study the vibration of a transmission line with an attached Stockbridge damper. They observed that asymmetric Stockbridge dampers were more effective at higher modes.

Many authors studied the forced vibration of transmission lines using methods based on impedance models. Tompkins et al.<sup>7</sup> examined the interaction of a conductor with a damper using the electrical-mechanical impedance method. That model was reformulated in solely mechanical-impedance terms by Rawlins<sup>8</sup> and then used to analyse conductor vibrations. Further extension of the model was proposed by Nigol and Houston<sup>9</sup> who included the boundary conditions at both ends and considered the arbitrary location of the excitation source. Their model was experimentally verified and it was used to demonstrate optimum damping concepts.

<sup>1</sup>College of Engineering and Technology, Central Michigan University, Mt Pleasant, MI, USA

<sup>2</sup>Department of Mechanical and Industrial Engineering, Ryerson University, Toronto, Ontario, Canada

### Corresponding author:

O Barry, Central Michigan University, ET 100, School of Engineering & Technology, Mt Pleasant, MI 48859, USA.  
Email: barrylo@cmich.edu

Energy balance method (EBM) is another method used to examine the forced-vibration analysis of transmission lines. The vibration level is evaluated by determining the balance between the energy imparted to the conductor by the wind and the energy dissipated by the conductor (via conductor self-damping) and the added dampers. Oliveira and Preire<sup>10</sup> developed a dynamical model of Aeolian vibration to predict the amplitude of steady-state motion of the conductor based on EBM. They included a method for solving the time-dependent Navier–Stokes equation. Kraus and Hagedorn<sup>11</sup> also employed the EBM to examine vibration magnitudes. Their results were compared to those obtained from a wind tunnel experiment. The optimal position of Stockbridge dampers along the span of the conductor was investigated by Verma and Hagedorn.<sup>12</sup> To avoid locating dampers on nodes for system natural frequencies of less than 50 Hz, they analytically showed that it was sufficient to maintain approximately 1 m maximum distance between adjacent dampers.

A major drawback of the impedance and EBM approaches is the limitation to only one-way coupling between the conductor and damper. Specifically, the dynamics of the damper influenced that of the conductor but not the converse. An attempt at modelling a two-way coupling scenario was reported in Barry et al.<sup>5,6,13,14</sup> The messenger cable and counterweights were modelled as two cantilevered Euler-Bernoulli beams with rigid tip masses. The system was connected to the conductor via a rigid link. While the efficacy of the model was demonstrated, it was very complicated compared with that based on EBM or the impedance method. It was also computationally intensive because of the numerous degrees of freedom employed. The present exposition addresses these shortcomings by replacing the continuum damper model with an equivalent discrete system.

The Stockbridge damper was reduced to an equivalent mass-spring-mass and viscous damping system. Hence, the transmission line system was modelled as an axially loaded Euler-Bernoulli beam with in-span mass-spring-mass and viscous damping system. Numerous researchers (see Lin and Tsai,<sup>15</sup> Ercoli and Laura,<sup>16</sup> Liu and Huang,<sup>17</sup> Wu and Lin,<sup>18</sup> Gurgoze<sup>19</sup> and Cha<sup>20</sup> and the references mentioned therein) have investigated the vibration of beams with an attached in-span mass and/or spring-mass system. In spite of these interests, there was no investigation where the beam was subjected to an axial

load while supporting an in-span mass-spring-mass and viscous damping system.

In developing the equivalent model, experiments were performed to determine the equivalent viscous damping using the forced response method. The equivalent mass and stiffness of the messenger were determined on the premise that the damper consisted of the two cantilevered beams with a tip mass. The equations of motion were derived using Hamilton principle. Explicit expressions were presented for the characteristic equation, and mode shapes. The model was validated using both the numerical and experimental results in the literature. Parametric studies were conducted to investigate the effect of the magnitude and location of the damper on the natural frequency. The role of the Strouhal frequency on the vibration response was also examined.

### Description of the system

A schematic of a single conductor with a Stockbridge damper is depicted in Figure 1. The Stockbridge damper comprised of a clamp, a messenger (or damper cable) and a mass (or counterweight) at each end of the messenger. The clamp, messenger and damper counterweights were modelled as cantilevered Euler-Bernoulli beams with tip masses, as shown in Figure 2. The damper was reduced to an equivalent spring-mass and viscous damping system. The conductor and the Stockbridge damper were finally reduced to an equivalent tensile beam with an in-span mass-spring-mass and viscous damping system (see Figure 3). The additional in-span mass represented the mass of the clamp  $M_c$ . The equivalent viscous damping was determined experimentally (as outlined in the following section). Since the Stockbridge damper can be modelled as two independent cantilever beams each with a tip mass, the equivalent stiffness,  $k$ , is then the parallel combination of the stiffnesses of the two cantilevered beams. The equivalent

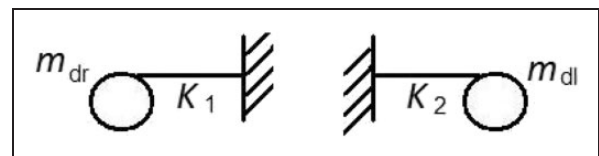


**Figure 2.** Schematic of Stockbridge damper messenger with counterweight.

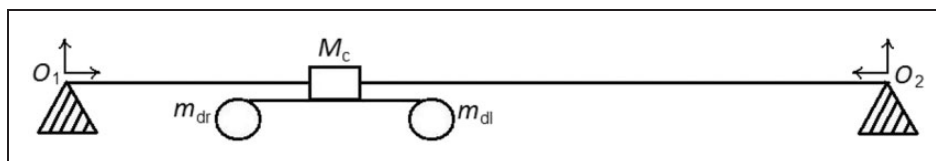


**Figure 1.** Schematic of a single conductor with a Stockbridge damper.

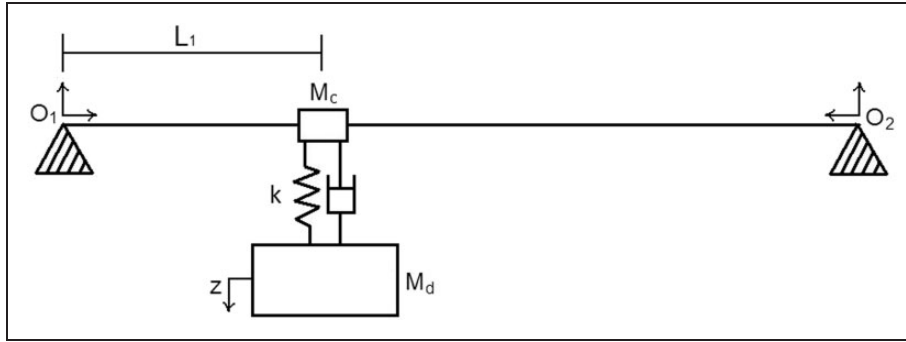


**Figure 3.** Schematic of a simply supported beam with an in-span mass-spring-mass system.

mass,  $M_d$  is the sum of equivalent mass of a cantilever beam and the mass of the counterweight on each side.

Assuming that all the wires bend together, the theoretical maximum bending stiffness of the conductor and messenger are calculated to be  $E_c I_c = 1602 \text{ Nm}^2$  and  $E_m I_m = 31.8 \text{ Nm}^2$ , respectively.

$$k = 2 \left( \frac{3E_m I_m}{L_m^3} \right) \quad (1)$$

$$M_d = \frac{33m_m L_m}{140} + m_{dr} + m_{dl} \quad (2)$$

where  $E_m I_m$  and  $m_m$  are the messenger flexural rigidity and mass per unit length, respectively. The masses of the right-hand side and left-hand side ends of the messenger are denoted by  $m_{dr}$  and  $m_{dl}$ , respectively.  $L_m$  denotes the total length of the messenger.

## Experiments

The Stockbridge damper is often postulated as non-linear because it is dependent upon the forcing frequency and the conductor vibration amplitude at the location of the damper clamp.<sup>9,21–23</sup> The nonlinearity of the damper can be modelled as an equivalent viscous damping.<sup>24</sup> This equivalent damping coefficient  $c_d$  is estimated from empirical data as:

$$c_d = \frac{E_d \omega}{\pi V_c^2} \quad (3)$$

where

$$E_d = \frac{P_d}{f} \text{ and } P_d = \frac{1}{2} F V_c \cos \phi_{FV} \quad (4)$$

$\omega$  is the circular frequency in rad/s.  $E_d$  and  $P_d$  are the energy and power dissipated by the damper over a complete cycle, respectively;  $f$  is the excited frequency in Hz,  $F$  is the force transmitted to the shaker by the damper,  $V_c$  is the measured velocity at the clamp, and  $\phi_{FV}$  is the phase angle between the force and the velocity.

The experimental investigation was conducted by means of the forced response method to measure the force transmitted to the shaker by the damper, the velocity of the clamp, and the phase angle between the velocity and the force. The experimental procedure and set-up were performed according to IEEE std.664.<sup>25</sup> The schematic of the experimental set-up is depicted in Figure 4. The Stockbridge damper was mounted on an electrodynamic shaker (Bruel & Kjaer 4802). A load cell (Dytran 1061V1) was installed between the shaker and the fixture to measure the delivered force and an accelerometer (B&K 4382) was placed at the clamp to measure the velocity of the damper.

The characteristics of the Stockbridge damper are as follows: the flexural rigidity is  $E_m I_m = 31.8 \text{ Nm}^2$  and mass per unit length is  $m_m = 0.25 \text{ kg/m}$ . The mass of the right and left counterweights are  $m_{dr} = 3.4 \text{ kg}$  and  $m_{dl} = 1.46 \text{ kg}$ . The length of the messenger on the right and left are  $L_L = 0.22 \text{ m}$  and  $L_R = 0.3 \text{ m}$ .

The Stockbridge damper was excited in the range of wind-induced vibration (sweep) at a constant velocity 100 mm/s. The frequency range was confined to frequencies greater than 10 Hz, given that the shaker was not applicable to frequencies lower than 10 Hz. Both load cell and accelerometer were connected to a dynamic signal analyzer (PCI-6034E) through charge amplifiers (Dytran 4115 and B&K 2635). For each tested frequency, values were recorded for the input force from the shaker, velocity at the clamp, and phase angle between the force and the velocity. The recorded frequency, force and velocity at the clamp are employed in equation (3) to obtain the equivalent damping coefficient of the Stockbridge damper. A plot of  $c_d$  against the recorded frequencies is shown in Figure 5. It indicates that the equivalent viscous damping increases up to certain peaks and then decreases. It should be noted that the frequencies corresponding to these peaks are the resonant frequencies of the Stockbridge damper.

## Equations of motion

Two reference frames were attached at the ends of the conductor as shown in Figure 3. The damper was

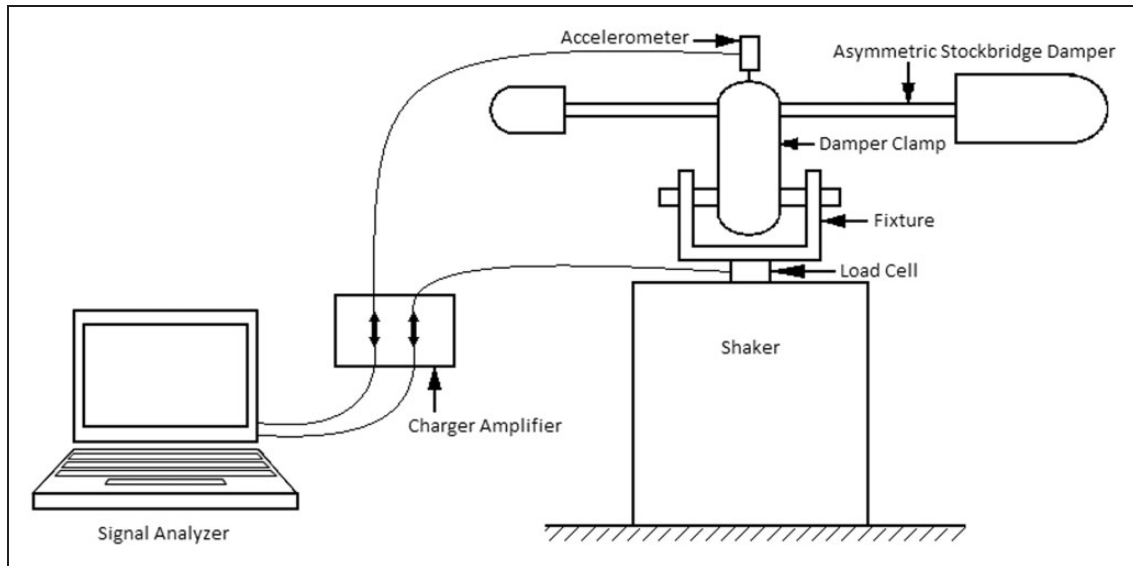


Figure 4. Schematic of the experimental set-up.

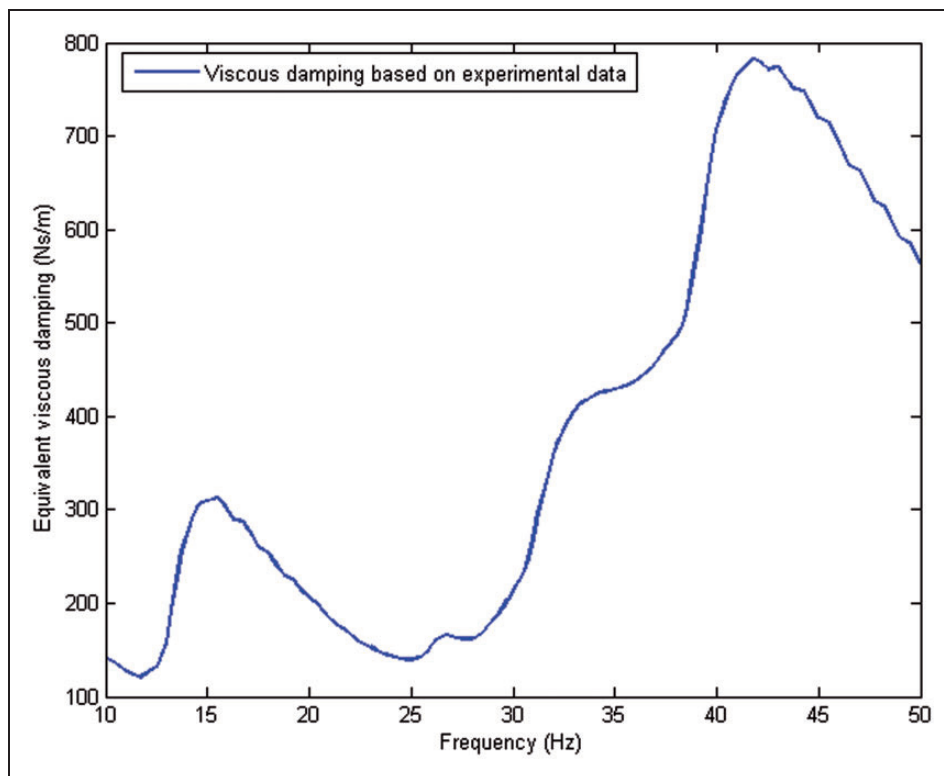


Figure 5. Equivalent viscous damping coefficient of the Stockbridge damper.

located at a distance  $L_1$  from the left-hand side reference frame, and the conductor was deemed as being divided into two segments. The transverse displacement of each segment was measured relative to the appropriate reference frame, and it is denoted by  $w_i(x_i, t)$  for  $i = 1, 2$ . The vertical displacements of the mass attached to the conductor  $M_c$  and the suspended mass  $M_d$  are denoted by  $z_0(t)$  and  $z(t)$ ,

respectively. The system kinetic  $\mathcal{T}$  and potential  $\mathcal{V}$  energy may then be expressed as

$$\mathcal{T} = \frac{1}{2}m_c \sum_{i=1}^2 \int_0^{L_i} \dot{w}_i^2(x, t)dx + \frac{1}{2}M_d \dot{z}^2 + \frac{1}{2}M_c \dot{z}_0^2 \tag{5}$$

$$\mathcal{V} = \frac{1}{2} E_c I_c \sum_{i=1}^2 \int_0^{L_i} w_i''^2(x, t) dx + \frac{1}{2} c_d (\dot{z} - \dot{z}_0)^2 + \frac{1}{2} k (z - z_0)^2 + \frac{1}{2} T \sum_{i=1}^2 \int_0^{L_i} w_i'^2(x, t) dx \tag{6}$$

where  $z_0(t) = w_1(L_1, t)$ ,  $E_c I_c$  is the conductor flexural rigidity,  $m_c$  is mass per unit length of the conductor and  $T$  denotes the conductor pretension. The overdots and primes denote temporal and spatial derivatives, respectively.

These energies were introduced into the Hamilton's principle. The continuity equations and the resulting coupled system governing equations and boundary conditions may be written as

$$E_c I_c w_i'''' + m_c \ddot{w}_i - T w_i'' = 0 \tag{7}$$

$$M_d \ddot{z} + c_d (\dot{z} - \dot{z}_0) + k (z - z_0) = 0 \tag{8}$$

$$M_c \ddot{z}_0 - E_c I_c w_1''(L_1, t) + T w_1'(L_1, t) + c_d (\dot{z}_0 - \dot{z}) + k (z_0 - z) - E_c I_c w_2''(L_2, t) + T w_2'(L_2, t) = 0 \tag{9}$$

$$w_1(L_1, t) = w_2(L_2, t) \tag{10}$$

$$w_1'(L_1, t) = -w_2'(L_2, t) \tag{11}$$

$$w_1''(L_1, t) = w_2''(L_2, t) \tag{12}$$

$$w_1(0, t) = w_1''(0, t) = w_2(0, t) = w_2''(0, t) = 0 \tag{13}$$

**Free vibration**

Assuming the system exhibits harmonic vibration such that the deformations  $w_i(x_i, t)$  and displacements  $z(t)$  were expressed as

$$w_i(x, t) = L W_i(\zeta_i) e^{j\omega t} \quad \text{for } i = 1, 2 \tag{14}$$

$$z(t) = L Z e^{j\omega t} \tag{15}$$

where  $j = \sqrt{-1}$ ,  $W_i(\zeta_i)$  and  $Z$  are the respective non-dimensional amplitudes of  $w_i(x_i, t)$  and  $z(t)$ , and  $\omega$  is the circular natural frequency of the system. Substituting the above equations into equations (7)–(13), and ignoring viscous damping component, yielded the following non-dimensional system equations:

$$W_i''''(\zeta_i) - s^2 W_i''(\zeta_i) - \Omega^4 W_i(\zeta_i) = 0 \tag{16}$$

$$Z - K W_1(\xi_1) = 0 \tag{17}$$

$$W_1''(\xi_1) - s^2 W_1'(\xi_1) - \eta W_1(\xi_1) + \gamma Z = -W_2'''(\xi_2) + s^2 W_2'(\xi_2) \tag{18}$$

$$W_1(\xi_1) = W_2(\xi_2) \tag{19}$$

$$W_1'(\xi_1) = -W_2'(\xi_2) \tag{20}$$

$$W_1''(\xi_1) = W_2''(\xi_2) \tag{21}$$

$$W_1(0) = W_1''(0) = W_2(0) = W_2''(0) = 0 \tag{22}$$

where

$$\xi_1 = \frac{L_1}{L}, \quad \xi_2 = \frac{L - L_1}{L}, \quad K = \frac{k}{k - M_d \omega^2}, \quad s^2 = \frac{T L^2}{E_c I_c} \tag{23}$$

$$\Omega^4 = \frac{m_c \omega^2}{E_c I_c} L^4, \quad \eta = \frac{k - \omega^2 M_c}{E_c I_c} L^3, \tag{24}$$

$$\gamma = \frac{k L^3}{E_c I_c} \quad \text{and} \quad \zeta_i = \frac{x_i}{L}$$

The general solution of equation (16) for each beam or conductor segment was expressed as

$$W_i = c_{i1} \sin \alpha \zeta_i + c_{i2} \cos \alpha \zeta_i + c_{i3} \sinh \beta \zeta_i + c_{i4} \cosh \beta \zeta_i \tag{25}$$

where

$$\alpha = \sqrt{-\frac{s^2}{2} + \sqrt{\frac{s^4}{4} + \Omega^4}} \quad \text{and} \quad \beta = \sqrt{\frac{s^2}{2} + \sqrt{\frac{s^4}{4} + \Omega^4}} \tag{26}$$

For brevity, the following symbols  $s_i$ ,  $c_i$ ,  $sh_i$  and  $ch_i$  were introduced to denote  $\sin \alpha \xi_i$ ,  $\cos \alpha \xi_i$ ,  $\sinh \alpha \xi_i$  and  $\cosh \alpha \xi_i$ , respectively. Hence the characteristic (or frequency) equation may be written as

$$(k - \omega^2 M_d)(-\beta \eta \alpha^2 c_{\alpha\theta} sh_\beta + \alpha \eta \beta^2 s_\alpha ch_\beta - \alpha \eta \beta^2 s_\alpha ch_{\beta\theta} - \alpha \beta^2 \gamma K s_\alpha ch_\beta + \alpha \beta^2 \gamma K s_\alpha ch_{\beta\theta} + \beta \eta \alpha^2 c_\alpha sh_\beta - \beta \gamma K \alpha^2 c_\alpha sh_\beta - \alpha^3 \gamma K s_\alpha ch_\beta + \alpha^3 \gamma K s_\alpha ch_{\beta\theta} - \beta^3 \gamma K c_\alpha sh_\beta + \beta^3 \eta c_\alpha sh_\beta - 2\alpha \beta^5 s_\alpha sh_\beta - 2\alpha^5 \beta s_\alpha sh_\beta - \beta^3 \eta c_{\alpha\theta} sh_\beta - 4\alpha^3 \beta^3 s_\alpha sh_\beta + \alpha^3 \eta s_\alpha ch_\beta - \alpha^3 \eta s_\alpha ch_{\beta\theta} + \beta \gamma K \alpha^2 c_{\alpha\theta} sh_\beta + \beta^3 \gamma K c_{\alpha\theta} sh_\beta) = 0 \tag{27}$$

where

$$\phi = c_1 \alpha^3 + s_1 (\eta - \gamma K) \tag{28}$$

$$\epsilon = -ch_1 \beta^3 + sh_1 (\eta - \gamma K) \tag{29}$$

$$\kappa = c_2 \alpha^3 \tag{30}$$

$$\chi = -ch_2 \beta^3 \tag{31}$$

$c_\alpha = \cos \alpha$ ,  $c_{\alpha\theta} = \cos(\alpha\{\xi_1 - \xi_2\})$ ,  $s_\alpha = \sin \alpha$ ,  $ch_\beta = \cosh \beta$ ,  $sh_\beta = \sinh \beta$ , and  $ch_{\beta\alpha} = \cosh(\beta\{\xi_1 - \xi_2\})$ . The characteristic equation is multiplicatively decomposed into a component that yielded the natural frequency of the suspended simple discrete spring-mass system and another that provided the frequency of the more complex system. The shape functions are now written as

$$W_1(\zeta_1) = c_{11} \sin \alpha \zeta_1 \tag{32}$$

$$W_2(\zeta_2) = c_{11} \frac{s_1}{s_2} \sin \alpha \zeta_2 \tag{33}$$

**Forced vibration**

Given that the validation of the forced response was based on the experiment reported in Nigol and Houston,<sup>9</sup> the excitation force was from the mid-span located at the electrodynamic shaker. This force can be expressed as  $F(x, t) = f(t)\delta(\zeta - 0.5)$ , and the forced-vibration equations may be written as

$$m_c \ddot{w} + E_c I_c w^{IV} - T w'' + \delta(x - L_1) [M_c \ddot{w} + k(w - z) + c_d(\dot{w} - \dot{z})] = F(x, t) \delta\left(x - \frac{L}{2}\right) \tag{34}$$

$$M_d \ddot{z} + k(z - w(L_1)) + c_d (\dot{z} - \dot{w}(L_1)) = 0 \tag{35}$$

The solutions of equations (34) and (35) were obtained using mode superposition principle. The deflection of the beam was assumed as

$$w(x, t) = L \sum_{i=1}^{\infty} W_i(\zeta) q_i(t) \tag{36}$$

$$z(t) = LZ_i q_i(t) \tag{37}$$

where  $q_i(t)$ s are the generalized displacements and  $W_i(\zeta)$  are the mode shapes

Substituting equations (36) and (37) into equations (34) and (35), then projecting onto the  $j$ th eigenfunction and using the classical orthonormality conditions, the following equation was obtained

$$\ddot{q}_j + c_j \dot{q}_j + \omega_j^2 q_j = Q_j \quad \text{for } j = 1, 2, \dots \tag{38}$$

where  $\omega_j$  is the system natural frequency and  $c_j$  and  $Q_j$  are given as

$$c_j = \frac{c_d}{\mu_j m_c L} (W_{1j}(\xi_1) - Z_j)^2 \tag{39}$$

$$Q_j = \frac{1}{\mu_j m_c L} F(x, t) W_{2j} \quad (\zeta_2 = 0.5) \tag{40}$$

and

$$\mu_j = \int_0^{\xi_1} W_{1j}^2 d\zeta_1 + \int_0^{\xi_2} W_{2j}^2 d\zeta_2 + \frac{1}{mL} \left( W_{1j}^2(\xi_1) M_c + Z_j^2 M_d \right) \tag{41}$$

Equation (38) was solved using Runge-Kutta numerical integration method, and the vibration response of the conductor and the damper were determined using equations (36) and (37), respectively.

**Numerical simulation**

The free vibration analyses were based on a 795-KCMIL-DRAKE-ACSR conductor with the following parameters: conductor diameter  $d_c = 28.1$  mm, flexural rigidity  $E_c I_c = 1602$  Nm<sup>2</sup>, mass per unit length  $m_c = 1.6286$  kg/m, and the tension  $T = 27,840$  N. The Stockbridge damper data were provided in ‘Experiments’ section. The parameters of the equivalent reduced model were: suspended mass  $M_d = 4.83$  kg, clamp mass  $M_c = 0.2$  kg and equivalent spring stiffness  $k = 1356.96$  N/m.

The first 10 natural frequencies are tabulated in Table 1 for a given conductor length of 27.25 m. The results in the second column were obtained using equation (27), the frequency equation. The third column represents the results obtained via a FE implementation of the conductor and mass-spring-mass model. A good agreement was observed between the values of the exact solution and the FE method. This observation is true for the results in Barry et al.,<sup>5</sup> which are presented in the fourth column. The second natural frequency was not captured in Barry et al.<sup>5</sup> This frequency, 16.5798 rad/s, was in close proximity

**Table 1.** The first 10 natural frequencies obtained using various methods for conductor in-span mass  $M_c = 0.2$  kg,  $L = 27.25$  m and damper location  $\xi_1 = 0.05$ .

Mode	Natural frequency (Hz)			
	Present	Finite element	Barry et al. <sup>5</sup>	Bare beam
1	2.3845	2.3845	2.3981	2.4011
2	2.6384	2.6387	–	4.8077
3	4.8164	4.8164	4.7820	7.2252
4	7.2337	7.2337	7.1263	9.6593
5	9.6663	9.6663	9.3843	12.1150
6	12.1182	12.1182	11.5202	14.5980
7	14.5942	14.5943	13.6375	17.1132
8	17.0992	17.0994	15.9025	19.6657
9	19.6385	19.6389	18.3324	22.2607
10	22.2172	22.2181	20.8802	24.9027

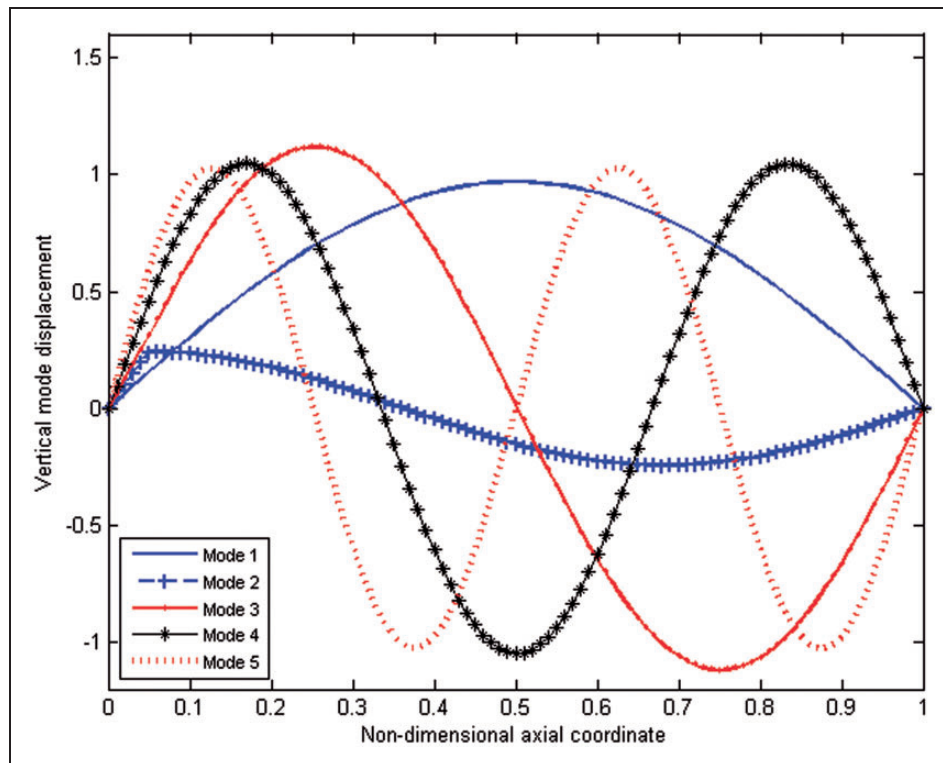


**Figure 6.** The mode shapes corresponding to the lowest five natural frequency of the conductor with mass-spring-mass system.

to that of the suspended spring-mass system (i.e.  $\omega = \sqrt{\frac{k}{M_d}} \approx 2.6674$  Hz), and its absence may be explained by their formulation method. The damper employed in Barry et al.<sup>5</sup> was as a system comprising two independent beams that were cantilevered to a rigid link which was connected to the conductor. Each cantilevered beam modelled a segment of the messenger and carried a tip mass which represented the counterweight. The bare beam frequencies were obtained by using equation (27) and setting the  $M_d$ ,  $M_c$  and  $k$  to be zero.

A plot of the mode shapes corresponding to the lowest five mode shapes of the system is depicted in Figure 6. Except for the second mode shape, these mode shapes can be related to the mode shapes of the bare beam. As observed earlier, the second mode frequency was in the proximity of the natural frequency of the suspended spring-mass system. It is conjectured that the inertia/mass of the damper effectively divided the conductor into two segments.

For a given conductor length of 200 m, the influences of the relative magnitudes of the in-span mass  $M_c$  and the suspended mass  $M_d$  on the system natural frequencies were examined by maintaining their total sum constant – in the reported simulation  $M_c + M_d = 5$  kg. The results are tabulated in Table 2. Using the scenario where the two masses are equal as a reference, it was observed that increasing the in-span mass  $M_c$  (and simultaneously decreasing the suspended mass  $M_d$  in order to maintain the constant total mass condition) increased the system natural frequencies of all five modes. This is plausible because

**Table 2.** The lowest five natural frequencies when the span length  $L = 200$  m, in-span mass-spring-mass system is located at  $\xi_1 = 0.0333$ , and the magnitudes of the in-span mass  $M_c$  and suspended mass  $M_d$  are selected such that their sum  $M_c + M_d = 5$  kg.

Mass (kg) $M_c, M_d$	Natural frequency (Hz)				
	$f_1$	$f_2$	$f_3$	$f_4$	$f_5$
0, 5	0.3270	0.6536	0.9794	1.3035	1.6236
1, 4	0.3270	0.6536	0.9795	1.3040	1.6258
2, 3	0.3270	0.6536	0.9796	1.3043	1.6272
2.5, 2.5	0.3270	0.6536	0.9796	1.3044	1.6276
3, 2	0.3270	0.6536	0.9796	1.3045	1.6280
4, 1	0.3270	0.6536	0.9796	1.3047	1.6284
5, 0	0.3270	0.6536	0.9796	1.3047	1.6286

increasing the in-span mass effectively increased the system stiffness (via the segmentation).

Figure 7 shows the effect of the damper location on the system natural frequencies. The frequency at each damper location was normalized with respect to the frequency corresponding to the damper location  $\xi_1 = 0.004$ . The normalizing frequencies were 2.0548, 4.1096, 6.1645, 8.2195 and 10.2746 rad/s, corresponding to modes 1 through 5, respectively. One half of the conductor length is plotted because of symmetry. The first mode decreased monotonically with decreasing distance of the damper from the conductor midpoint. This is because the effective stiffness of the system decreases as the damper location approaches

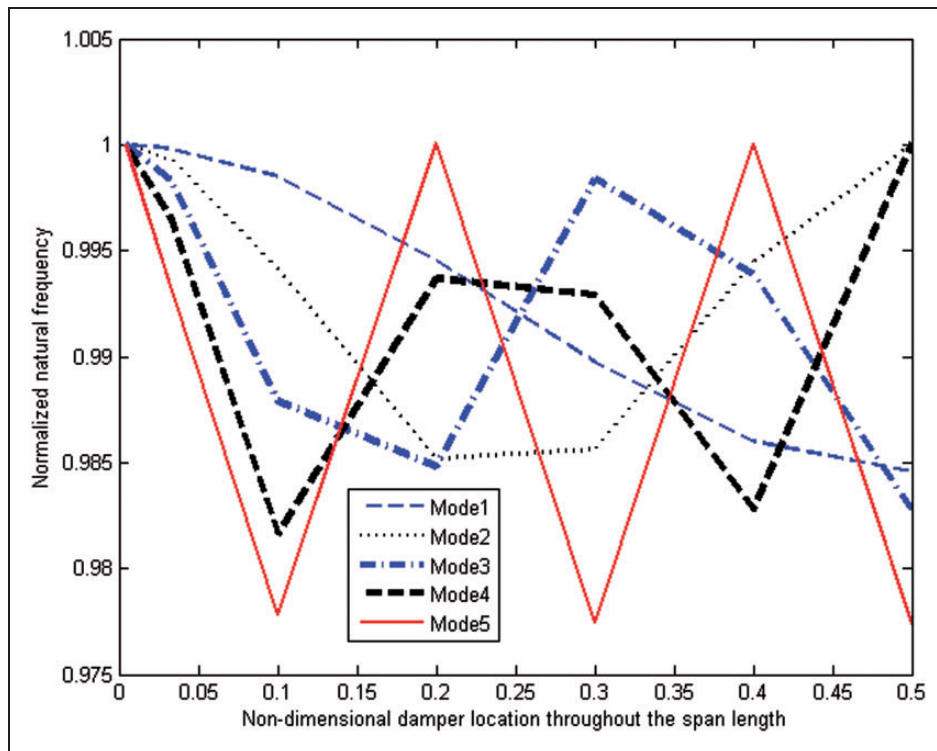


**Figure 7.** The effect of the damper location on natural frequencies for span length  $L = 200$  m. The frequencies are non-dimensionalized as  $\frac{\omega_i}{\omega_{\xi=0.004}}$ .

the centre of the conductor. The other four modes were remarkably affected in that they all decreased and increased depending on whether they were approaching a node or an anti-node. The rate of change was more pronounced in the fifth frequency.

With regard to forced vibration analysis, the validation of the present model was examined in threefold: the first and second employed the indoor experimental data reported in Nigol and Houston<sup>9</sup> and Barry et al.,<sup>14</sup> respectively. The third relied on the FE model of Barry et al.<sup>6</sup> In the case of the first indoor experiment, a 585 Kcmil (26/7) ASCR conductor was strung between two rigid terminals that were 23.5 m apart. Two identical dampers were attached at a distance of 1.73 m from each end and a shaker was mounted at mid-span. The shaker force and the mid-span velocity of the conductor were measured for various resonant frequencies. The tested conductor had the following characteristics: diameter  $d_c = 24.1$  m, mass per unit length  $m_c = 1.19$  kg/m, rated tensile strength (RTS) of 105 kN. The tested damper was a single degree-of-freedom damper and it comprised a mass  $M_d = 3.19$  kg, spring stiffness  $k = 3800$  N/m, and an equivalent viscous damping  $c_d = 177$  Ns/m. A conductor tension of 25% RTS was considered. The experimental results were based on the optimum curve depicted in Figure 11 of Nigol and Houston.<sup>9</sup> The proposed model was also extended to accommodate the attachment of two dampers. Further, the mass of the clamp was ignored in order to properly represent the tested damper. The

comparison of the experimental data and the computed results from the proposed model are presented in Figure 8. They show very good agreement. It should be noted that the ratio of velocity over excitation force was measured and computed at the point of excitation.

The second part of the validation consisted of the indoor experiment reported in Barry et al.<sup>14</sup> The conductor 795 Kcmil ASCR was strung between two rigid terminals 27.25 m apart and one Stockbridge damper with the same parameters described in 'Experiments' section. The results are depicted in Figure 9. Albeit the present model tends to overestimate the vibration amplitude for frequency higher than 20 Hz, it shows similar trends to the model employed in Barry et al.<sup>14</sup> That is both models capture the vibration level of the conductor very well.

The third part of the validation and the rest of the numerical analyses were also based on the 795 Kcmil ASCR conductor and the Stockbridge damper data provided in the experimental section. The system was subjected to a concentrated harmonic force  $f(t) = F_0 \sin(\Omega_f t)$  N. The equivalent viscous damping was obtained from Figure 5 for each excitation frequency. Figure 10 depicts plots of the conductor non-dimensional maximum vibration amplitude for various Strouhal frequencies which were obtained using both the proposed model and that in Barry et al.<sup>6</sup> In reference to the conductor vibrational response, the results obtained using the present model were in good agreement with those obtained

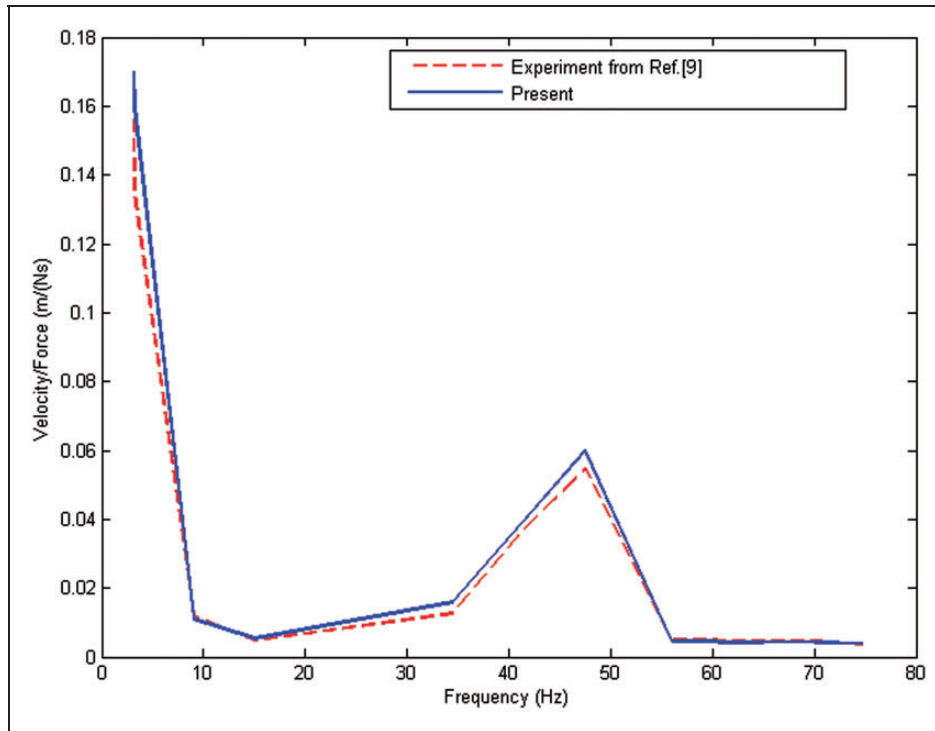


**Figure 8.** Validation of the proposed model via experiment with one degree freedom damper ( $L = 23.5$  m,  $L_1 = 1.73$  m,  $L_2 = 21.77$  m,  $c_d = 177$  Ns/m).

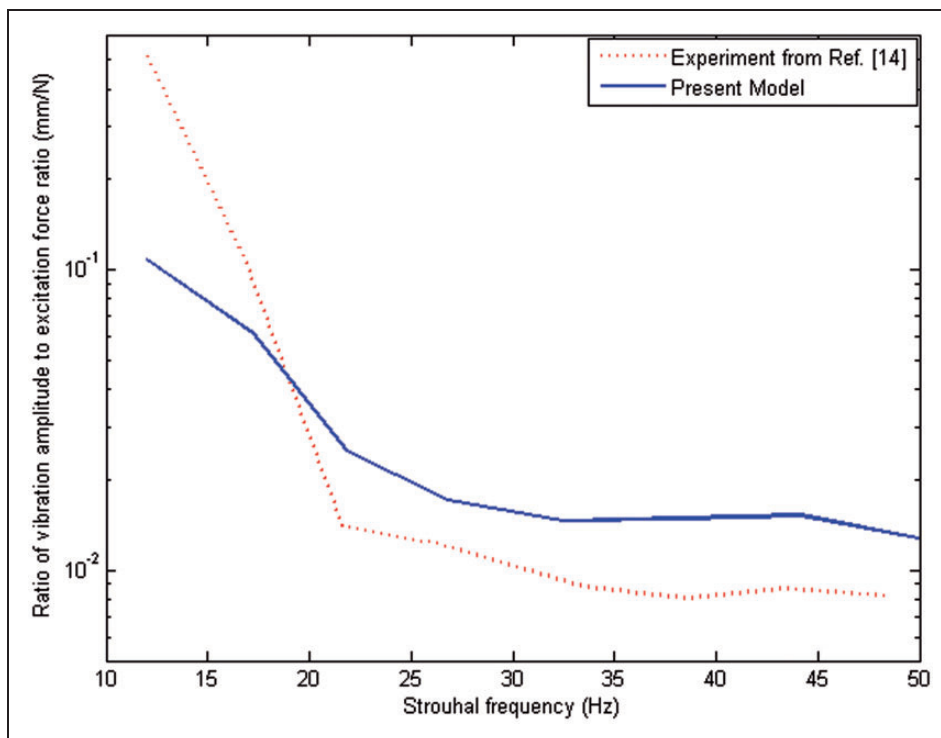


**Figure 9.** Validation of the proposed model via experiment with Stockbridge damper ( $L = 27.25$  m and  $L_1 = 0.94$  m).

using Barry et al.<sup>6</sup> The normalized mid-span vibration amplitude of the conductor (relative to the conductor diameter,  $d$ ) decreased with increasing forcing frequency. The results for the damper showed poor agreement with those obtained using the FE

method. This poor agreement between the proposed simple model and the complete, but complicated model of Barry et al.,<sup>6</sup> indicates that the former cannot be used to predict the response of the counterweights.

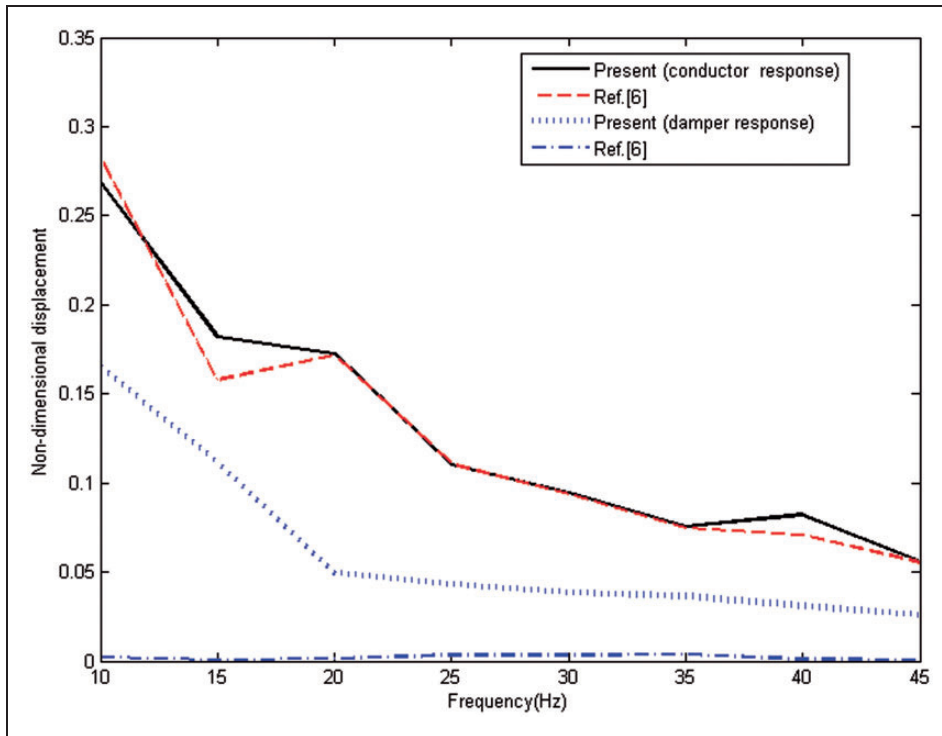


Figure 10. Validation of the proposed model via finite element ( $L = 200$  m,  $L_1 = 3.33$  m,  $F_0 = 100$  N).

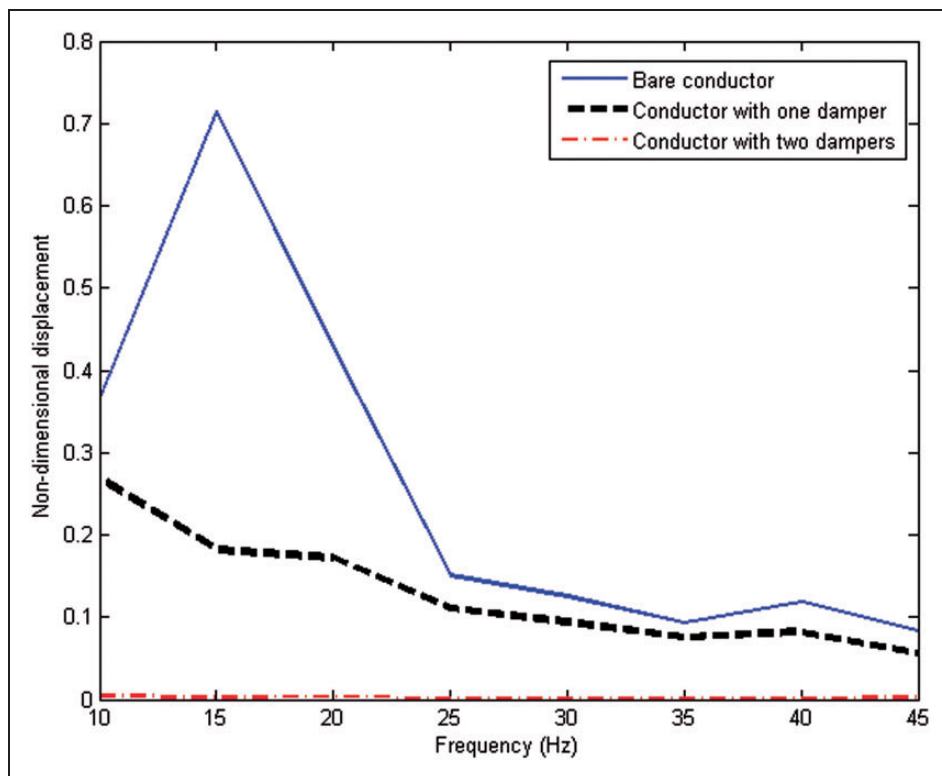
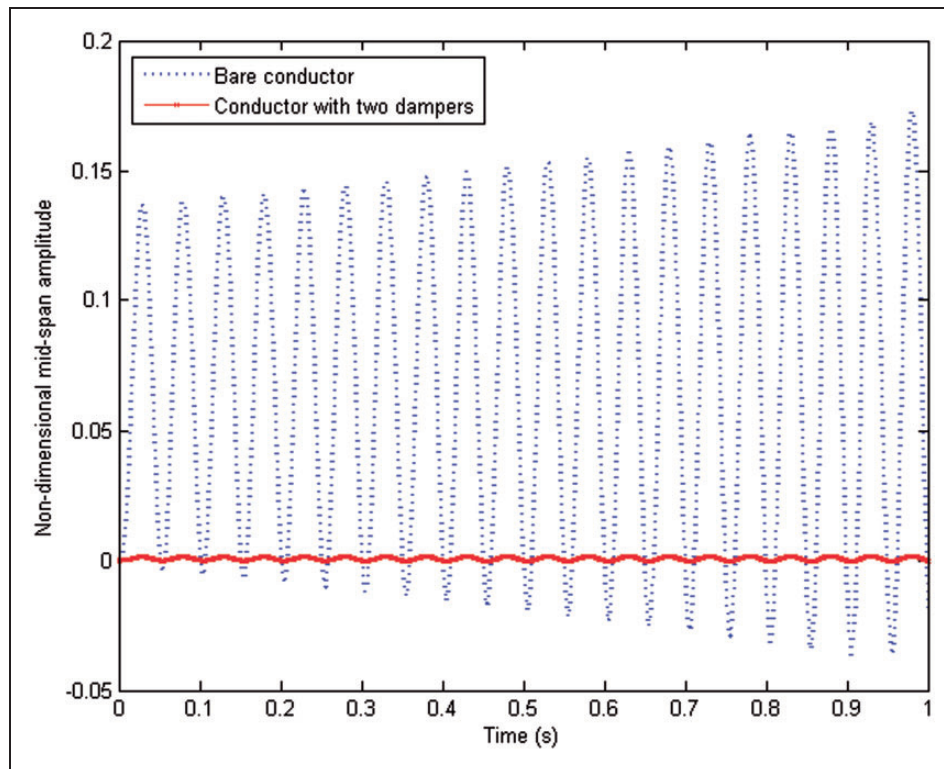


Figure 11. The effect of attaching dampers ( $L = 200$  m,  $L_1 = 3.33$  m,  $F_0 = 100$  N).

The effect of attaching one or two dampers on the conductor is demonstrated in Figure 11. Three plots of the non-dimensionalized mid-span vibration amplitude are depicted. The first plot is that of the bare

conductor, second is for one damper at  $L_1 = 3.33$  m, and third for two dampers at 3.33 m from each end. The results indicated that using one damper reduced the vibration of the conductor, and the reduction was



**Figure 12.** The bare and loaded conductor non-dimensional vibration amplitude ( $L = 200$  m,  $L_1 = 3.33$  m,  $L_2 = 193.67$  m,  $F_0 = 100$  N,  $f = 20$  Hz).

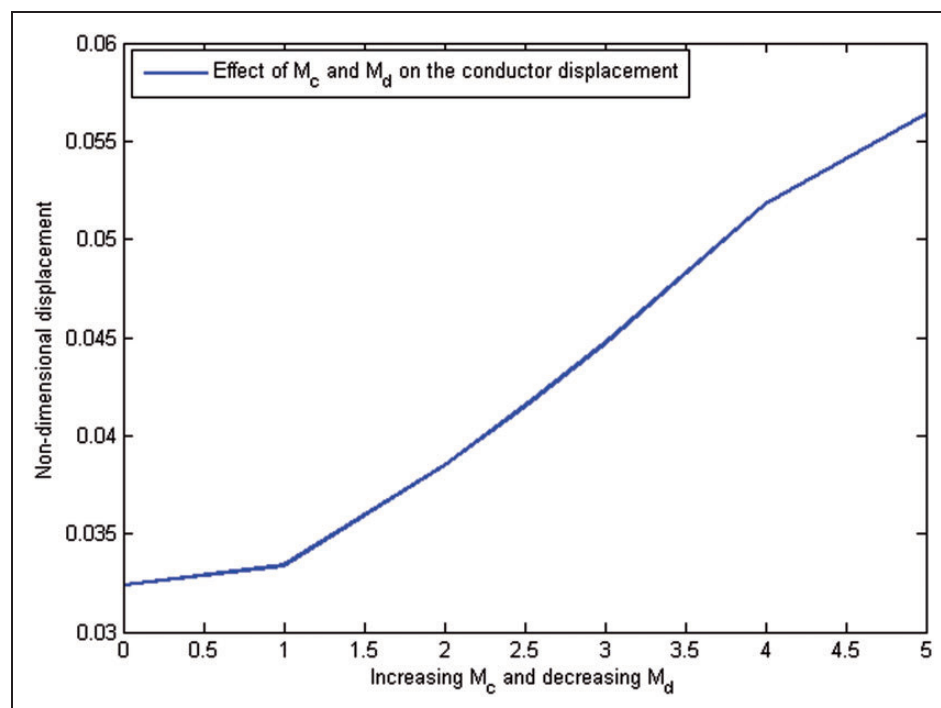


**Figure 13.** Effect of  $M_c$  and  $M_d$  on the vibration response of the conductor ( $L = 30$  m,  $c_d = 300$  Ns/m,  $f = 15$  Hz,  $F_0 = 10$  N).

most pronounced between 10 and 25 Hz. With two dampers, the vibration of the conductor was drastically reduced throughout the whole range of forcing frequency. To further illustrate the role of attaching two dampers, Figure 12 depicts plots of vibration

response of the bare and loaded conductor for a given forcing frequency of 20 Hz. The response of the bare conductor displays a resonance phenomenon as expected because the forcing frequency was closer to one of the system natural frequencies.

This resonance was completely eliminated in the system with two dampers.

In Figure 13, the effect of the relative magnitudes of the in-span mass  $M_c$  and the suspended mass  $M_d$  on the system response were examined. This was done by increasing  $M_c$  from 0 to 5 and simultaneously decreasing  $M_d$  from 5 to 0 kg while maintaining their total sum constant. The results show an increase in the conductor displacement. This implies that the suspended mass has more effect for dampening the conductor than the in-span mass.

## Conclusion

The free and forced vibration responses of a single conductor equipped with Stockbridge dampers were examined. The damper was reduced to an equivalent discrete mass-spring-mass and viscous damping system. The viscous damping of the Stockbridge damper was determined experimentally. The system equations of motion were derived using Hamilton's principle. Explicit expressions were presented for the frequency (or characteristic) equation, and mode shapes. The validity of the formulation was demonstrated via comparisons with experimental results and FE numerical method results. The proposed simple model was effective for predicting the conductor response and natural frequencies of the system (i.e. combined conductor and damper), but a poor predictor of the response of the counterweights. The numerical simulations showed significant dependency of the natural frequencies on damper location and total mass. This was more pronounced when the damper was in the proximity of antinodes. With regard to the forced vibration, increasing the forcing frequency significantly reduced the vibration amplitude of the conductor. The use of two dampers was significantly superior to using one damper.

## Declaration of Conflicting Interests

The author(s) declared no potential conflicts of interest with respect to the research, authorship, and/or publication of this article.

## Funding

The author(s) disclosed receipt of the following financial support for the research, authorship, and/or publication of this article: The authors thank Central Michigan University for the financial support of this research project.

## References

1. Electrical Power Research Institute, Inc. *Transmission line reference book: wind-induced conductor motion*. Palo Alto, CA: EPRI, 2006, 618 p.
2. Claren R and Diana G. Mathematical analysis of transmission line vibration. *IEEE Trans Power Appl Syst* 1969; 60: 1741–1771.
3. Dhotard MS, Ganesan N and Rao BVA. Transmission line vibration. *J Sound Vib* 1978; 60: 217–237.
4. Barbieri N, de Souza OH and Barbieri R. Dynamical analysis of transmission lines cables, part 1 – linear theory. *Mech Syst Signal Process* 2004; 18: 659–669.
5. Barry O, Oguamanam DCD and Lin DC. Free vibration analysis of a single conductor with a Stockbridge damper. In: *23rd Canadian Congress of Applied Mechanics (CANCAM) proceedings*, Vancouver, British Columbia, June 2011, pp.944–946.
6. Barry O, Oguamanam DCD and Lin DC. Aeolian vibration of a single conductor with a Stockbridge damper. *Proc IMechE, Part C: J Mechanical Engineering Science* 2012; 227. DOI: 10.1177/0954406212452064.
7. Tompkins JS, Merrill LL and Jones BL. Quantitative relationships in conductor vibration using rigid models. *IEEE Trans Power Appl Syst* 1956; 75: 879–896.
8. Rawlins CB. *Recent developments in conductor vibration*. Aluminum Company of America, 1958, Alcoa Technical Paper Issue 13. 32 p.
9. Nigol O and Houston HJ. Aeolian vibration of single conductor and its control. *IEEE Trans Power Appl Syst* 1985; 104: 3245–3254.
10. Oliveira RE and Preire DG. Dynamical modeling and analysis of Aeolian vibration of single conductors. *IEEE Trans Power Deliv* 1994; 9: 1685–1693.
11. Kraus M and Hagedorn P. Aeolian vibration: wind energy input evaluated from measurements on an energized transmission lines. *IEEE Trans Power Deliv* 1991; 6: 1264–1270.
12. Verma H and Hagerdorn P. Wind induced vibration of long electrical overhead transmission line spans: a modified approach. *J Wind Struct* 2005; 8: 89–106.
13. Barry O. *Finite element modeling of a single conductor with a Stockbridge damper under Aeolian vibration*. MASC Thesis, Ryerson University, Toronto, Ontario, 2010 January.
14. Barry O, Zu JW and Oguamanam DCD. Forced vibration of overhead transmission line: analytical and experimental investigation. *J Vib Acoust* 2014; 136. DOI: 10.1115/1.4027578.
15. Lin HY and Tsai YC. Free vibration analysis of a uniform multi-span beam carrying multiple mass spring-mass systems. *J Sound Vib* 2007; 302: 442–456.
16. Ercoli L and Laura PAA. Analytical and experimental investigation on continuous beams carrying elastically mounted masses. *J Sound Vib* 1987; 114: 519–533.
17. Liu WH and Huang CC. Free vibration of restrained beam carrying concentrated masses. *J Sound Vib* 1988; 123: 31–42.
18. Wu JS and Lin TL. Free vibration analysis of a uniform cantilever beam with point masses by an analytical-and-numerical-combined method. *J Sound Vib* 1990; 136: 201–213.
19. Gurgoze M. On the eigenfrequencies of a cantilever beam with attached tip mass and spring-mass system. *J Sound Vib* 1996; 190: 149–162.
20. Cha PD. Natural frequencies of a linear elastica carrying any number of sprung masses. *J Sound Vib* 2001; 247: 185–194.
21. Vecchiarelli J, Curries IG and Havard DG. Computational analysis of Aeolian conductor vibration with a Stockbridge-type damper. *J Fluid Struct* 2000; 14: 489–509.
22. Havard DG. Weakness in the forced response method for testing vibration dampers. *IEEE Standard 664* 1994.

23. Barry O, Zu JW and Oguamanam DCD. Nonlinear dynamics of Stockbridge dampers. *J Dyn Syst Meas Control* 2015; 137. DOI: 10.1115/1.4029526.
24. Bandstra JP. Comparison of equivalent viscous damping and nonlinear damping in discrete and continuous system. *J Vib Acoust* 1983; 105: 382–392.
25. Guide on the measurement of the performance of Aeolian vibration dampers for single conductors. *IEEE Standard 664*, 1980. DOI: 10.1109/IEEESTD.1980.81009.

## Appendix

### Notation

$c_d$	equivalent damping coefficient
$d_c$	diameter of conductor
$E_c I_c$	flexural rigidity of conductor
$E_d$	energy dissipated by damper
$E_d I_d$	flexural rigidity of damper
$f$	excitation frequency
$F$	applied force
$k$	equivalent damper stiffness
$L$	length of conductor

$L_1$	damper location on the conductor
$L_m$	length of messenger
$L_L$	length of left messenger
$L_R$	length of right messenger
$m_c$	mass per unit length of conductor
$M_c$	mass of clamp
$M_d$	equivalent mass of damper
$m_{dl}$	mass of right damper
$m_{dr}$	mass of left damper
$m_m$	mass per unit length of messenger
$P_d$	power dissipated by damper
$q(t)$	generalized displacement
$T$	tension of conductor
$\mathcal{T}$	kinetic energy
$V_c$	measured velocity of damper clamp
$\mathcal{V}$	potential energy
$w(x,t)$	transverse displacement of conductor
$W(\zeta)$	mode shape
$z(t)$	vibration displacement of conductor
$\phi_{FV}$	phase angle between force and velocity
$\omega$	circular frequency